Estimation of Snow Parameters Based on Passive Microwave Remote Sensing and Meteorological Information

Final Report
NASA Grant NAGW 4251

March 15, 1995–July 15, 1996

by

Leung Tsang
Principal Investigator
Department of Electrical Engineering, Box 352500
University of Washington, Seattle, WA 98195

and

Jenq-Neng Hwang
Co-Principal Investigator
Department of Electrical Engineering, Box 352500
University of Washington, Seattle, WA 98195

submitted to

Dr. Ming Ying Wei
NASA Headquarters
Water Cycle Processes Program, Code SEP
Office of Space Science and Applications
Earth Science and Applications Division
6000 Independence Avenue SW
Washington, DC 20546

Abstract

A method to incorporate passive microwave remote sensing measurements within a spatially distributed snow hydrology model to provide estimates of the spatial distribution of snow water equivalent (SWE) as a function of time is implemented. The passive microwave remote sensing measurements are at 25 km resolution. However, in mountain regions the spatial variability of SWE over a 25 km footprint is large due to topographic influences. On the other hand, the snow hydrology model has built-in topographic information and the capability to estimate SWE at a 1 km resolution. In our work, the snow hydrology SWE estimates are updated and corrected using SSM/I passive microwave remote sensing measurements. The method is applied to the Upper Rio Grande River Basin in the mountains of Colorado. The change in prediction of SWE from hydrology modeling with and without updating is compared with measurements from two SNOTEL sites in and near the basin. The results indicate that the method incorporating the remote sensing measurements into the hydrology model is able to more closely estimate the temporal evolution of the measured values of SWE as a function of time.

1. Introduction

Mountain seasonal snowpacks provide much of the potable water supply in many areas, particularly the western United States. These mountain snowpacks exhibit high spatial variability in their properties, especially snow water equivalent (SWE), which is an important variable in hydrology and water resources engineering. The total water content of the snow and its spatial distribution determine the amount and timing of snow meltwater available for water supply and hydropower generation. The development of a method to estimate spatial distributions of snow properties such as SWE at a 1 km spatial resolution will provide information useful to snow melt prediction.

The estimation of distributed SWE, however, remains a challenge due to the high variability of this quantity over small distances. Point measurements of snow properties, such as the SNOTEL (SNOwpack TELemetry) measurements of SWE are sparsely distributed and not representative of the parameter spatial variability. This makes it difficult to obtain a sufficiently accurate estimate of the water volume available in the snowpack and

to incorporate these measurements into basin-scale spatially distributed hydrology models which operate on a spatial grid of resolution 1 km or less.

Satellite remote sensing appears to have the potential for overcoming this deficiency due to its inherent ability to measure spatial averages of snow properties. By their nature, satellite remote sensing measurements can provide spatial estimates of snow properties and are suited as inputs to spatially distributed hydrologic models. There has been previous success in using satellite remote sensing measurements for the determination of snow properties. The most successful has been the delineation of snow covered area (SCA) using either visible (Dozier and Marks, 1987) or microwave (Josberger and Beauvillain, 1989) satellite measurements. The estimation of liquid water in the snowpack using microwave radar measurements has also shown some success when compared with field measurements (Shi and Dozier, 1995). The capabilities of satellite derived SCA within a snow hydrology model has been shown (i.e., Rango, 1988). More information on snow remote sensing and its applications within snow hydrology models can be found in the recent reviews of Rango (1993), Engman (1995), and Bales and Harrington (1995).

Passive microwave remote sensing should also be able to provide information on other snow properties. The received microwave signal from the earth's surface is dependent on snow properties such as grain size, temperature, depth, and density. Unlike the use of SCA within hydrology models, less has been done in fully exploiting this information with a snow hydrology model. Rango et al. (1989) and Chang et al. (1991) have explored the use of passive microwave remote sensing measurements to obtain basin-wide estimates of SWE. Examinations of the relation between snow properties and passive microwave brightness temperatures have been undertaken (see for example Hallikainen and Jolma, 1992; Wang et al., 1992), but the relationship is not direct and estimation of snow properties remains difficult. One of the difficulties in implementing a direct estimation technique for snow properties is the many-to-one inverse problem encountered in going from the measured microwave brightness temperatures to the snowpack properties. Another problem is the difference in spatial resolution between a spatially distributed hydrology model (1 km, or less) and the footprint resolution of the passive microwave measurements (25 km). Thus, these previous algorithms retrieve averaged snow parameters over the 25 km footprint.

To tackle these problems we use a method that combines several elements: a spatially distributed snow hydrology model, a snow-microwave radiative transfer model, and a parameter estimation technique with error minimizing steepest descent gradient

search. The spatial hydrology model operates at a 1 km pixel resolution using point meteorological measurements as forcings and outputs snowpack parameters at this resolution. Based on the snow property outputs, a microwave scattering model is used to determine the brightness temperatures for each pixel. The 1 km pixel estimates are integrated to the footprint measurement resolution and compared with the measured SSM/I brightness temperatures. The adjusted brightness temperatures are disaggregated to the pixel level and inverted to give new snow parameters used as updating inputs to the snow hydrology model. The hydrology model continues running until the next update.

To test this method, we apply it to a hydrological basin in the mountains of Colorado. The estimates of the temporal evolution of SWE are compared to SNOTEL ground truth measurements at two sites.

2. Methodology

The methodology outlined in the introduction section consists of combining several sources of information to provide the best estimate of the snowpack state parameters as possible. We use a spatially distributed snow hydrology model and microwave satellite measurements. These are linked by a snow-microwave scattering model and a parameter estimation technique. In this section the new algorithm is outlined with each component discussed in greater detail in the next section. The procedure used in obtaining the spatial snow water equivalent estimates is given in the flow chart of Figure 1. Each step is denoted by a letter in the flow chart and corresponds to the lettered description below.

a) The spatial data files are input to the snow hydrology model to determine the pixel characteristics of the model grid at 1 km resolution. The hourly point meteorological station information is used to drive the energy balance component of the snow hydrology model. These measurements consist of air temperature, dew point temperature, surface pressure, precipitation, cloud cover, and wind speed. These forcing variables are needed as input for each pixel and are adjusted for each pixel based on its topographic characteristics.

b) Net energy fluxes are calculated for each pixel using the snowpack surface energy balance model which operates at a 1 km spatial resolution. The output from the snow

hydrology model is snow depth, density, grain size, and temperature. These parameters are determined for each pixel on an hourly basis.

c) At the end of each day, the four output snowpack parameters are saved for use as input to the remote sensing-electromagnetic scattering model. The end-of-day values coincide with the nighttime satellite measurements used.

d) Based on the snowpack parameters obtained from the snow hydrology model, the brightness temperature estimates at 1 km spatial resolution are made. This is done for 19 and 37 GHz for both vertical and horizontal polarizations. Each is integrated to the 25 km scale to match the scale of the satellite measurements.

e) SSM/I measurements, with a resolution of 25 km, are used to compare with those obtained from the models. The area of coverage is determined for each remote sensing measurement; this is the overlap between the spatial domain of the models and the field of view of the sensor measurements.

f) The differences between the spatially averaged simulated brightness temperatures and those measured by the sensor are determined for each coverage area. The differences are uniformly distributed back to each individual pixel in the respective coverage area. Each pixel is adjusted by the same difference so that the average value of the pixel brightness temperatures for the coverage area equals the values obtained from the SSM/I measurements.

g) Snow parameters at the pixel (1 km) scale are determined from the adjusted brightness temperatures through inversion. The updated snow parameters are returned to the snow hydrology model which moves forward in time until the next available nighttime sensor observation, whereupon the process repeats itself.

Our algorithm is a systematic combination of hydrology model and remote sensing measurements. The remote sensing measurements are used to update and correct the hydrology model prediction. On the other hand, the hydrology model constrains the parameter inversion from the remote sensing measurements. This solves the many-to-one inverse problem in remote sensing, as the hydrology model gives *a priori* estimates of the snow parameter inversion. In addition, this algorithm gives snow parameter products at 1 km resolution as well as the temporal evolution of snow parameters.

The available data is discussed in the next section. Due to a lack of ground truth, we implement this algorithm only for selected points where measurements of snow water equivalent are available. This is used to validate the algorithm and demonstrate that the

algorithm has the potential to provide snow parameter estiates at the 1 km pixel resolution. Thus, we have not implemented the 25 km integration of step (e) and all of step (f).

3. Data Characteristics

The basin chosen for the application of the technique is the upper portion of the Rio Grande River in the mountains of Colorado. The basin is defined by the streamgauge at Del Norte, Colorado and has an area of 3419 km^2 with an elevation range of 2432–4215 m. This basin has been used for previous snow-remote sensing studies (e.g., Rango et al., 1989; Chang et al., 1991). The location of the basin is shown in Figure 2. We use the 1992–1993 snow year for the application. We employ several data types in the implementation and validation of the new algorithm: hydrology inputs, remote sensing measurements, and ground truth. These are discussed below and listed in Table 1.

A. Hydrology model inputs

The data used to run the hydrology model consists of topographic and weather data. The basin topographical characteristics are determined from 30 arc-second digital elevation model (DEM) output, which gives an approximate pixel resolution of 1 km and defines the spatial grid of the hydrology model. The basin area and its topographic representation are determined from the DEM and shown in Figure 3. From the DEM file, pixel elevation is determined, and slope, aspect, and shading characteristics of the pixels are calculated.

The forest cover plays an important role in the energy and mass balances of the snowpack through the reduction of shortwave radiation and wind speed, and the interception of snowfall by the forest canopy. Thus it is important to include forest cover information in the snow hydrology model. Pixel forest cover was determined from the Land Use and Land Cover digital files from the U.S. Geological Survey (USGS, 1990), which uses a classification scheme developed by Anderson et al. (1976). The land use pixels, with 200 m resolution, are aggregated to the DEM pixel scale (1 km) and used to determine whether each hydrology model pixel is open, forested, or some fraction thereof.

The snow hydrology model uses meteorological inputs to determine the precipitation characteristics as well as drive the snowpack surface energy balance. Hourly point meteorological measurements from the National Weather Service are used in conjunction with a distribution scheme based on the topography to provide spatial inputs to

the snow hydrology model. These consist of air temperature, wind speed, relative humidity, cloud cover, and precipitation. Information from additional sites that record daily precipitation totals is also used. Additionally, U.S. Geological Survey daily streamflow values at the outlet of the basin are used to estimate the volume of precipitation over the basin.

B. Satellite remote sensing measurements

Defense Meteorological Satellite Program (DMSP) Special Sensor Microwave Imager (SSM/I) brightness temperatures are obtained from the Distributed Active Archive Center (DAAC) at the Marshall Space Flight Center. The SSM/I measures microwave emission at four frequencies: 19, 22, 37 and 85 GHz with dual-polarization, except at 22 GHz, which is vertical only. More information on this sensor can be found in Hollinger et al. (1990). We selected the F8 satellite, using the brightness temperature measurements at the 19 and 37 GHz frequencies with horizontal and vertical polarizations, providing four different measurements for each footprint. Each day with measurements over the basin is determined. The nighttime measurements are saved and the daytime measurements are discarded due to the possibility of small amounts of liquid water present in the snowpack as a result of slight surface melting during the day, which re-freezes at night.

While the orbit of the satellite is sun-synchronous, providing approximately the same time of coverage over the basin, there are some days for which there is no satellite coverage of the basin. Additionally the footprint positions vary slightly from day to day. This means that the relationship between the satellite footprint that covers a pixel and the pixel snow properties is not constant since the distribution of pixels within the footprint changes. The change in footprint location for a SNOTEL pixel (#4) over four consecutive days is shown in Figure 4. This effect must be taken into account when attempting to relate pixel values of snow properties with the brightness temperature measurements of the satellite footprint and will be discussed further in a later section.

C. Ground truth measurements for algorithm validation

The SNOTEL measurement network records daily SWE values at selected points throughout the mountains of the western United States. Six of these stations are located within or very near the Upper Rio Grande basin for the year of study. Their names, locations, and elevations are listed in Table 2 and their locations with respect to the basin shown in Figure 3 (as indicated by an 'X'). The stations are all in the upper area of the

basin where the snow amounts are larger and measurements more important. For this study, the SNOTEL values are taken as representing the SWE for the 1 km pixel within which it lies. These measurements represent the ground truth to evaluate the performance of and validate the algorithm.

4. Implementation of Methodology

The basic idea of combining snow hydrology information with passive microwave remote sensing measurements through parameter estimation techniques was outlined in a previous section. There are several ways of implementing the three major components of this algorithm. Several different types of snow hydrology models and microwave radiative transfer models are available. Additionally there are several possible approaches to the parameter estimation procedure of error minimization. We have chosen the following ways to implement the three components previously discussed.

A. Snow hydrology model

The snow model contains several components: accumulation, snow surface energy balance, and internal snowpack physics. Snowmelt runoff is not currently considered since we investigate only the accumulation portion of the snow season. The model operates on a spatial grid of resolution approximately 1 km as determined by the DEM. Hourly meteorological inputs are input to the snow hydrology model to drive the accumulation and surface energy balance components. These inputs are adjusted for each model pixel using an elevation relationship such as air temperature lapse rate, $dT_a/dz = \text{constant}$.

The variables describing the snowpack for use in the radiative transfer model are snow depth d, snowpack temperature T_s, grain size (radius) g_s, and fractional volume f_s. These four variables are referred to as the snowpack state variables S. Each pixel within the spatially distributed snow hydrology model will have its own set **S**. The snow hydrology model maintains two related snowpack state variables: snow density ρ_s and snow water equivalent W. These are related to the parameters in **S** by

$$\rho_s = 0.91 f_s, \tag{1}$$

and

$$W = \rho_s \cdot d, \tag{2}$$

where 0.91 is the assumed density of ice ($g \cdot cm^{-3}$) and W is in cm. These state variables evolve over time as a function of the mass and energy balances as discussed below.

The model operates over a discrete time step Δt, during which the snowpack water equivalent evolves according to

$$W(t + \Delta t) = W(t) + P - M - E, \tag{3}$$

where P is snowfall, M is melt, and E is the loss due to sublimation, all in units of cm.

The accumulation component of the model, P, is based on point precipitation and temperature records in the area, to determine the amount that falls and whether it falls as rain or snow. The precipitation/elevation relationship is adjusted using the SNOTEL data by adjusting the total volume of precipitation at the point. The total annual volume of precipitation over the basin is adjusted using the streamflow measurements.

Following Marks (1988) we use a two-layer snowpack model, which consists of an "active layer" from which melt is produced, and a secondary layer which contains the remainder of the snow. The active layer is chosen to have a depth of 10 cm, thus capturing most of the depth of solar radiation penetration (approximately 90 percent), while not requiring an unduly large amount of heat to initiate melt conditions. The melt from the active layer is

$$M = \frac{Q_n - Q_{cc}}{L_m}, \tag{4}$$

where L_m = 79.7 $cal \cdot g^{-1}$ is the latent heat of melt (the amount of energy required to transform ice to water), Q_n is the net energy flux into the snowpack, and Q_{cc} is the cold content of the active layer, representing the amount of heat necessary to raise its temperature to 0°C. If $Q_{cc} > Q_n$, then no melt occurs. Since the model only considers the accumulation and ablation process, the meltwater is immediately removed from the snowpack without any routing, and the possibility of the meltwater refreezing in the pack is not considered.

The snowpack cold content is

$$Q_{cc} = -C_s W T_s, \tag{5}$$

where C_s = 0.5 $\text{cal} \cdot \text{g}^{-1} \cdot \text{deg}^{-1}$ is the snowpack specific heat. If the net energy into the snowpack is great enough to raise the snowpack temperature to 0°C ($Q_n \geq Q_{cc}$) then melt will be produced according to (4). If no melt is produced, the updated snowpack temperature is

$$T_s(t + \Delta t) = \frac{Q_n}{C_s W} + T_s(t). \tag{6}$$

The mass loss due to sublimation is calculated as

$$E = \frac{Q_e}{L_s}, \tag{7}$$

where Q_e is the latent heat transfer from the energy balance and L_s = 677 $\text{cal} \cdot \text{g}^{-1}$ is the latent heat of sublimation (the amount of energy required to transform ice to vapor).

The net energy flux at the surface, Q_n, is given by

$$Q_n = Q_s + Q_l + Q_h + Q_e, \tag{8}$$

where the fluxes Q_s, Q_l, Q_h, Q_e are respectively shortwave, longwave, sensible, and latent heat. The ground-to-snowpack and the precipitation-to-snowpack heat transfers are small relative to the other terms of (8) and are thus omitted.

The equations used to estimate the components of the snow surface energy balance are based on the point model from Marks (1988). However, it has been generalized to a spatial model incorporating the topography and forest cover characteristics of the basin. This includes accounting for the topographical and vegetative effects on solar and longwave radiation. More information on the computation of the different components in the surface energy balance (Equation 8) is in Appendix A. SWE outputs are compared with the SNOTEL stations to determine that they are reasonably close.

The snowpack physics algorithms, which describe the evolution of snowpack properties such as snow grain size and density are taken from the SNTHERM model of

Jordan (1991). The snow metamorphism is driven by the outputs from the energy and mass balances previously discussed. The algorithms are simplified to operate for a one-layer snowpack; there is no variability in the vertical direction.

The equation for the evolution of snow grain size is

$$g_s(t+\Delta t) = 0.14\frac{g_2}{4g_s(t)}\Delta t + g_s(t), \tag{9}$$

where g_2 is an empirical constant with a value of $4.0\times10^{-8}\,\mathrm{m}^2\cdot\mathrm{s}^{-1}$.

There are two components in the snow compaction process: destructive metamorphism and overburden. Destructive metamorphism is important initially when snow density is less than 0.15 $\mathrm{g}\cdot\mathrm{cm}^{-3}$. For dry snow, the empirical function used for compaction is

$$\left|\frac{1}{\Delta z}\frac{\partial \Delta z}{\partial t}\right|_m = -2.778\times10^{-6}\times c_3\times c_4\times\exp\left[-0.04(273.15-\mathrm{T})\right], \tag{10}$$

where c_4 is 1 for dry snow (the case here) and

$$c_3 = 1 \qquad \text{if} \qquad \rho_s \le 0.15\ \mathrm{g}\cdot\mathrm{cm}^{-3},$$
$$c_3 = \exp\left[-46.\cdot(\rho_s - 0.15)\right] \qquad \text{if} \qquad \rho_s > 0.15\ \mathrm{g}\cdot\mathrm{cm}^{-3}.$$

After snow has undergone its initial settling stage, densification proceeds at a slower rate determined mainly by compaction due to snow overburden pressure P_s such that

$$\left|\frac{1}{\Delta z}\frac{\partial \Delta z}{\partial t}\right|_o = -\frac{P_s}{\eta_0}\exp\left[-c_5(273.15-T)\right]\exp\left(-c_6\cdot\rho_s\right), \tag{11}$$

where η_0 is a viscosity coefficient for snow and c_5 and c_6 are constants based on observational evidence. The compaction rate is thus the combination of these two terms. As the depth changes but the water equivalent does not (no melt), the density of the snowpack will also change.

The final output of four snowpack parameters for the microwave scattering model is: d snow depth, T_s snowpack average temperature, g_s snowpack average grain size, and

f_s snowpack average fractional volume, $\mathbf{S} = \{d, T_s, g_s, f_s\}$. These four snowpack parameters serve as the link between the microwave scattering model and the snow hydrology model.

Figure 5 shows the comparison between the hydrology model output SWE and the measured SWE for two SNOTEL stations: #2 which is a high elevation station and #4 which is a low elevation station. The model is able to reproduce the snowfall events, but is usually not able to accurately reproduce the amounts. This is due to the simple scheme used to determine snowfall amounts in a topographically complex area. This is where the incorporation of information from passive microwave remote sensing measurements can improve SWE estimates.

To demonstrate the evolution of these parameters in time, simulation outputs from the hydrology model for all four snow parameters at station #2 (Figure 6a–d) and station #4 (Figure 7a-d) are shown. In both cases the depth increases whenever there is a snowfall event, then decreases as the snow compacts. Snowpack temperature stays low until the end of March, when it starts to increase as the melt season approaches. Grain radius and fractional volume both follow nearly the same shape of curve. This is due to the averaging of the snowpack properties to one layer. These values increase as the snowpack metamorphoses, until a new snowfall event, which reduces the average snowpack value by introducing fresh snow, which has smaller grain sizes and is less dense.

B. Snow-microwave radiative transfer

In passive microwave remote sensing the microwave emission from the ground surface is measured. This radiation is attenuated by the snowpack as a function of its temperature, depth, density, and grain size, as well as liquid water. To avoid the complications due to liquid water in the snowpack we use only nighttime measurements, when the snowpack has re-frozen, and do not continue the snow simulation into the melt season. From the snow hydrology model of the previous section, we have estimates of the four snowpack parameters **S** at the pixel scale. The brightness temperatures at this 1 km scale can be estimated using a microwave scattering model. Thus, from the model we have the brightness temperature vector $\mathbf{T_b} = \{T_{b_{19V}}, T_{b_{19H}}, T_{b_{37V}}, T_{b_{37H}}\}$, where 19 and 37 represent the frequency in GHz and V and H the vertical and horizontal polarization.

The model used to simulate the microwave interaction with the snowpack is the dense medium radiative transfer (DMRT) model (Tsang 1987, 1992). Unlike the traditional radiative transfer models, the DMRT takes into account the dependency of

scattering upon relative particle positions. This is important in a dense medium such as snow. The model incorporates a particle size distribution using a modified gamma distribution. Thus a medium containing particles of different sizes, such as snow, can be accounted for. The model accounts for scattering by particles as well as the interaction at the snow/soil interface and the snow/air interface. The equations describing the model are presented below. Additional details on the model and its implementation are in Tsang et al. (1992).

We consider thermal emission from a layer of dielectric particles of permittivity ε_s embedded in a background medium of permittivity ε overlaying a homogeneous half-space of dielectric medium of permittivity ε_2 (see Figure 8). Note for the case of snow, the background permittivity ε is ε_0 of free space and the particle permittivity ε_s will be that of ice. The particle sizes obey a size distribution $n(g)$ which is the number of particles per unit volume with radii between g and $g+dg$. The medium is of uniform temperature T. Then the dense media radiative equation for passive remote sensing assumes the following matrix form, for $0 \le \theta \le \pi$:

$$\cos\theta \frac{\partial}{\partial z}\bar{I}(z,\theta) = -\kappa_e \bar{I}(z,\theta) + \kappa_e(1-\tilde{\omega})CT\begin{bmatrix}1\\1\end{bmatrix} + \frac{3}{8}\kappa_e\tilde{\omega}\int_0^{\pi}\sin\theta'\mathbf{P}(\theta,\theta')\cdot\bar{I}(z,\theta')d\theta' \tag{12}$$

where

$$\bar{I}(z,\theta) = \begin{bmatrix} I_v(z,\theta) \\ I_h(z,\theta)\end{bmatrix} \tag{13}$$

and I_v, I_h are the vertical and horizontal specific intensities, respectively. Also in (12), $C = K_b K'^2/(\lambda^2 k^2)$, K_b is Boltzman's constant, λ is the free space wavelength, K' is the real part of the effective wave number in region 1, k is the free space wave number, $\tilde{\omega}$ is the albedo, and $\kappa_e = 2\,\mathrm{Im}(K)$ is the extinction rate of the specific intensity. In (12)

$$\mathbf{P}(\theta,\theta') = \begin{bmatrix} p_{11}(\theta,\theta') & p_{12}(\theta,\theta') \\ p_{21}(\theta,\theta') & p_{22}(\theta,\theta')\end{bmatrix} \tag{14}$$

where

$$p_{11}(\theta,\theta') = 2\sin^2\theta\sin^2\theta' + \cos^2\theta\cos^2\theta' \tag{15}$$

$$p_{12}(\theta,\theta') = \cos^2\theta \tag{16}$$

$$p_{21}(\theta,\theta') = \cos^2\theta' \tag{17}$$

$$p_{22}(\theta,\theta') = 1. \tag{18}$$

For $0 \le \theta \le \pi/2$, the boundary conditions for (12) at the air-snow interface, $z = 0$, are

$$I_v(z=0,\pi-\theta) = R_v(\theta) I_v(z=0,\theta) \tag{19}$$

and

$$I_h(z=0,\pi-\theta) = R_h(\theta) I_h(z=0,\theta), \tag{20}$$

and for the snow-ground interface, $z = -d$, they are

$$I_v(z=-d,\theta) = R_{vg}(\theta) I_v(z=-d,\pi-\theta) + \left(1 - R_{vg}(\theta)\right) C T_g \tag{21}$$

and

$$I_h(z=-d,\theta) = R_{hg}(\theta) I_h(z=-d,\pi-\theta) + \left(1 - R_{hg}(\theta)\right) C T_g, \tag{22}$$

where R_v, R_h, R_{vg}, and R_{hg} are reflectivities.

After (12) is solved subject to the boundary conditions of (19)–(22), the brightness temperatures in the direction θ_0, where $\theta_0 = \sin^{-1}(K' \sin\theta / k)$ is related to θ by Snell's law, in region 0 for vertical and horizontal polarizations are given by

$$\begin{bmatrix} T_{B_v}(\theta_0) \\ T_{B_h}(\theta_0) \end{bmatrix} = \frac{1}{C} \begin{bmatrix} (1 - R_v(\theta)) I_v(z=0,\theta) \\ (1 - R_h(\theta)) I_h(z=0,\theta) \end{bmatrix}. \tag{23}$$

The differences between the dense medium theory and the conventional radiative transfer theory are the calculations of K, the extinction rate κ_e, and the albedo $\overline{\omega}$ in terms of the physical parameters of the medium, which are represented by ε_s and the size distribution $n(g)$. These parameters are determined by using approximations of the Dyson and Bethe-Salpeter equations. The cross pair distribution functions of multiple particle sizes are calculated through the Percus-Yevick approximation (Percus and Yevick, 1958;

Baxter, 1970) that expresses the correlations of particle positions in terms of the size distribution $n(g)$.

Also it is necessary to consider the effects of surface roughness in the Fresnel reflectivities, especially when the snowpack is thin. Following Wang et al. (1983) we use two polarization mixing parameters, one for each interface. For the upper boundary, the air-snow interface, $z = 0$,

$$R_v(\theta) = \left[(1-Q)r_v(\theta) + Qr_h(\theta)\right] \tag{24}$$

and

$$R_h(\theta) = \left[(1-Q)r_h(\theta) + Qr_v(\theta)\right], \tag{25}$$

where Q is the mixing fraction between the two reflection polarizations for the snow-air interface and r_v and r_h are the Fresnel reflectivities with effective propagation constant K determined by

$$r_v(\theta) = \left| \frac{k^2\cos\theta - K'\left(k^2 - K'^2\sin^2\theta\right)^{1/2}}{k^2\cos\theta + K'\left(k^2 - K'^2\sin^2\theta\right)^{1/2}} \right| \tag{26}$$

and

$$r_h(\theta) = \left| \frac{K'\cos\theta - \left(k^2 - K'^2\sin^2\theta\right)^{1/2}}{K'\cos\theta + \left(k^2 - K'^2\sin^2\theta\right)^{1/2}} \right|. \tag{27}$$

In the lower boundary, at the snow-ground interface, $z = -d$,

$$R_{v_g}(\theta) = \left[\left(1-Q_g\right)r_{v_g}(\theta) + Q_g r_{h_g}(\theta)\right] \tag{28}$$

and

$$R_{h_g}(\theta) = \left[\left(1-Q_g\right)r_{h_g}(\theta) + Q_g r_{v_g}(\theta)\right], \tag{29}$$

with

$$r_{v_s}(\theta)=\left|\frac{\frac{\varepsilon_2}{\varepsilon_0}k_0{}^2\cos\theta-K'\left(\frac{\varepsilon_2}{\varepsilon_0}k_0{}^2-K'^2\sin^2\theta\right)^{1/2}}{\frac{\varepsilon_2}{\varepsilon_0}k_0{}^2\cos\theta+K'\left(\frac{\varepsilon_2}{\varepsilon_0}k_0{}^2-K'^2\sin^2\theta\right)^{1/2}}\right| \tag{30}$$

and

$$r_{h_s}(\theta)=\left|\frac{K'\cos\theta-\left(\frac{\varepsilon_2}{\varepsilon_0}k_0{}^2-K'^2\sin^2\theta\right)^{1/2}}{K'\cos\theta+\left(\frac{\varepsilon_2}{\varepsilon_0}k_0{}^2-K'^2\sin^2\theta\right)^{1/2}}\right|, \tag{31}$$

where k_0 is the free space wave number.

In this study we use a Rayleigh size distribution of snow particles (West et al., 1993) represented by

$$n(g)=\frac{\pi f g}{16\langle g\rangle^5}\exp\left(-\frac{\pi g^2}{4\langle g\rangle^2}\right), \tag{32}$$

where $\langle g\rangle$ is the mean radius and f is the fractional volume of all the particles. The fractional volume and the mean radius are defined by

$$f=\int_0^\infty \frac{4\pi}{3}g^3 n(g)dg \tag{33}$$

$$\langle g\rangle=\frac{\int_0^\infty g n(g)dg}{\int_0^\infty n(g)dg}. \tag{34}$$

The advantage of the Rayleigh size distribution is that there are only two parameters: f fractional volume, and $\langle g\rangle$ mean grain size.

The medium input physical parameters of the dense medium radiative transfer equations using the Rayleigh size distribution include the previous vector of four snowpack parameters from the hydrology model **S** and a set of fixed parameters describing the electromagnetic properties of the dense medium, **F**, necessary to implement the DMRT.

This fixed set F consists of:

1) the complex permittivity of the particles: $\varepsilon_{s_{19}} = (3.2 + i0.00025)\varepsilon_0$ and $\varepsilon_{s_{37}} = (3.2 + i0.001)\varepsilon_0$, for 19 and 37 GHz respectively,
2) the permittivity of the ground surface, ε_g,
3) the ground surface temperature T_g,
4) the two previously described polarization reflectivity mixing parameters, Q and Q_g, and
5) the maximum grain size in the grain size distribution of (32), $g_{\max}$.

It is necessary to estimate some of the physical parameters of the scattering model, such as the emissivity of the soil and its initial temperature. This is done by calibration, using the microwave brightness temperature measurements for October, right before any snow has fallen and is covering the ground. This provides a calibration for soil properties, which affect the microwave brightness temperatures throughout the year, although much less as the snow season progresses and the snowpack becomes deeper. This allows for the estimation of ε_g, T_g, and the roughness mixing parameters, Q and Q_g.

Additionally, the determination of snow microwave properties through calibration is necessary. The maximum and minimum limits need to be set for the snow particle size distribution. The minimum value is based on the initial grain size used for fresh snow. The maximum value evolves through time, just as the shape of the particle distribution evolves through time. The hydrology model grain size (g) is taken as the distribution mean. The upper limit must be periodically re-established since as the mean grain size from the hydrology model evolves (Equation 9), the snow grain size distribution evolves with the upper limit increasing as well. The need to update is based on visual inspection of the snow grain size output from the model, see Figures 6c and 7c. The fixed parameter vector F is $\{\varepsilon_s, \varepsilon_g, T_g, Q, Q_g, g_{\max}\}$.

From these parameters, the brightness temperatures of vertical and horizontal polarization at specified frequencies and observation angles can be calculated from the above equations. Using the snow parameter output, the brightness temperatures at 19 and 37 GHz for vertical and horizontal polarizations are obtained at the 1 km pixel scale. The efficient, approximate representation of the snow microwave radiative transfer model is described in Appendix B using a neural network representation.

C. Remote sensing data that overlap a pixel

At the end of each day for which there is basin coverage from the sensor, the DMRT is used to estimate the four microwave brightness temperatures from the four snowpack parameters at pixel resolution (1 km). The pixel brightness temperatures are then averaged to the footprint scale (25 km) for each measurement. The difference between the pixel integrated brightness temperatures and SSM/I measured brightness temperatures is distributed back to the pixels from which these adjusted 1 km brightness temperatures can be used to obtain adjusted snowpack parameters.

The critical point in the previously described procedure is in going from the 1 km scale to the 25 km scale and then back to the 1 km scale. The remote sensing measurements cover approximately a 25 km area and thus represent a spatial average of snow properties that may be quite heterogeneous. Depending on the location of the pixel with respect to the center of the footprint, the pixel-to-footprint measurement relationship can vary from day to day.

To examine the possible fluctuations in remote sensing measurements due to footprint position, we compared SNOTEL sites with brightness temperatures assigned to a pixel based on the degree of coverage. The was examined as well in Wilson et al. (1996). Figure 9a shows the brightness temperatures for a coverage area with radius of 12.5 km, the actual footprint size. Figure 9b shows the brightness temperatures using a coverage radius of 4.0 km from the footprint center. As the pixel of interest becomes nearer to the center of the footprint, it should be more closely related to the footprint measurement. From the figures we see that the amount of fluctuation is reduced as the distance from pixel to footprint center is reduced, showing more clearly the expected trend of decreasing brightness temperatures with increasing snow depth. This method is employed in determining what measurements to use in the updating procedure.

5. Results

The implementation shown in Figure 1 is now demonstrated. A comparison between the two methods of determining SWE is made. The first method is the distributed snow hydrology model run independently of the remote sensing information, relying only on the topographic information and point meteorological measurements. The second method is using the snow hydrology model, but replacing the parameter outputs with the

updated set based on the remote sensing brightness temperatures. To determine how well the combined model performs compared to using only the spatially distributed snow hydrology model, we examine the results of the SWE curves from the two methods at two SNOTEL sites (#2 and #4). The comparison is made for the snow season of 1992–1993. The simulation starts on October 1, 1992, which is the first day of the hydrologic water year. The SNOTEL measurements are taken as the ground-truth for each site, representing the 1 km pixel within which it lies.

The snow hydrology model is run first, independently of any remote sensing information, solely on the point meteorological forcings. Then the simulation is started with the remote sensing updating scheme. We start the updating when the SWE is greater than 5 cm so that the scattering of the microwave emission by the snow is significant. An update is made every five days. Linear interpolation is used between the brightness temperature observations that are used based on the previously discussed coverage criterion. In the time interval between updates, the two methods will follow each other since the SWE curves are dependent only on the precipitation estimates during the accumulation period. The methods will diverge only at the updating steps.

The first station examined is station #4. It is a lower elevation station at 2860 m with smaller amounts of snow and maximum SWE of 15 cm. Its snow accumulation season begins later in the season than much of the basin. The results of the comparison are shown in Figure 10. We also include in the figure the measured SNOTEL SWE. One of the brightness temperature measurements, 37H, is included for reference. However, we have used all four brightness temperature measurements for the inversion of the snow parameters. Table 2 show the values for the fixed parameter vector **F** for this station.

Since significant snow accumulation does not develop at this station until late December, the updating with remote sensing measurements is not started until December 28. Improvement is obtained from using the updating procedure. Not every point is closer to the SNOTEL measurements than that obtained by the snow hydrology model alone, but more often it is closer. The updating is able to help compensate for poor snowfall estimates in the snow hydrology model, such as Day 110. The results in the figure indicate that the hydrology model with remote sensing updating is generally closer to the SNOTEL ground truth.

Another test simulation is done for a high elevation station, #2, at 3420 m with larger amounts of snow and a SWE maximum of 40 cm. Note that a change in elevation of 500 m between stations 2 and 4 gives a corresponding change in SWE of over 100%,

highlighting the spatial variability of SWE in this region. The comparison results are shown in Figure 11. Again an improvement is obtained from using the updating scheme. The results in the figure indicate that the hydrology model with remote sensing updating is generally closer to the SNOTEL ground truth.

Between Day 70 and 75 a drastic drop is observed in measured brightness temperature. This is most probably due to the development of large grain sizes from a small melt event; the SNOTEL measurement drops temporarily during this time. This is one instance where it is important to recalibrate the DMRT, changing the upper grain size limit in the distribution. In general, every 15 days (after 3 updating events) the upper limit of the grain size g_{max} is recalibrated. Table 2 also shows values of the fixed parameter vector **F** for this site. The main difference is in the evolution of the grain size as evidenced by the differences in upper limit to the grain size distribution. The incorporation of the upper limit in the grain size distribution as a parameter in the neural network to avoid this recalibration is under research.

6. Conclusions

A method to combine passive microwave remote sensing measurements within a spatially distributed snow hydrology model to estimate the time evolution and spatial distribution of snow parameters has been presented. The method combines the information contained within the satellite microwave measurements with that obtained from the spatially distributed snow hydrology model. A spatially distributed snow hydrology model that uses spatial topographic inputs and point meteorological measurements to force the energy balance is combined with the SNTHERM model to obtain the four snowpack parameters for passive microwave remote sensing: snowpack density, depth, temperature, and grain size at a 1 km scale. The brightness temperatures for these 1 km snow parameters are estimated using the dense medium radiative transfer model. These are compared with the 25 km resolution satellite measurements and the differences distributed back to the 1 km scale brightness temperatures. The adjusted snowpack parameters are determined by inverting the DMRT.

The approach has enabled us to handle the two difficulties previously discussed: differences in spatial scale between the spatially distributed snow hydrology model (1 km) and remote sensing measurements (25 km), and the non-uniqueness of the inversion of the

remote sensing measurements. By implementing the 1 km resolution hydrology model we are able to relate the 1 km to the 25 km resolution SSM/I measurements with the DMRT and some estimation techniques. Inversion of the adjusted pixel brightness temperatures provides the adjusted snow parameters at the 1 km scale to update the snow hydrology state variables. Analysis of the satellite footprints is undertaken to determine effective pixel SWE relationships with degree of footprint coverage to that pixel.

The approach is demonstrated for two SNOTEL sites, making a comparison between the case with only the snow hydrology model and the case that includes remote sensing updating. In each case there was overall improvement in the ability of the model to reproduce the SNOTEL SWE measurements when the remote sensing measurements were included.

This methodology shows promising results in improving snow water equivalent amounts from snow hydrology models. This method can be easily extended to all pixels within the basin to map snow properties such as SWE. Additional remotely sensed types of information such as snow covered area can be incorporated within this framework. Bayesian updating techniques, which can provide better estimation are currently under investigation (Davis et al., 1995).

Appendix A

In this appendix the equations used to estimate the different components of the snow surface energy fluxes (Equation 8) are presented. These are for shortwave and longwave radiation, and latent and sensible heat.

A.1 Shortwave radiation

Three components are considered in the calculation of shortwave radiation: direct, D, diffuse, I, and sky reflected, R. Reflected radiation from neighboring slopes is neglected; an assumption that is justified for forested catchments, but would need to be retained in high alpine environments. The total shortwave radiation into the snowpack is

$$Q_S = I + D + R \tag{A.1}$$

Direct radiation is that part of the solar beam that is not depleted due to scattering or absorption. Diffuse radiation is the fraction of the beam that is scattered in the forward direction. The sky reflected component is radiation reflected from the surface to the sky and then back to the surface again. This can be a significant component of total downward solar radiation over snow-covered surfaces where the albedo is high and there is low cloud cover. Presuming that measurements of I, D, and R are not available, which is normally the case, the direct and diffuse terms can be estimated using the clear sky equations of Munro and Young (1982) with the cloud effect estimated based on Davies et al. (1975) and Davies and Idso (1979). The direct component of solar radiation received at a snow covered pixel is

$$I = I_o H(1-\alpha_s)\left[\psi_{O_3}\psi_{rs} - (1-\psi_w)\right]\psi_{da}\psi_{ds}\psi_C F_s \qquad \text{(A.2)}$$

where I_o is the direct solar radiation reaching the top of the earth's atmosphere, H is a topographic parameter accounting for pixel slope, aspect, and shading, α_s is the snow albedo, ψ is the transmissivity function for ozone absorption, Rayleigh scattering, water vapor absorption, aerosol absorption and scattering, and clouds (for subscripts O_3 , rs, w, da, ds, and C), and F_s is an interception factor for forest cover.

The diffuse radiation component is estimated assuming that the fraction of Rayleigh scattering in the forward direction is one half, and that the fraction of Mie scattering in the forward direction is 0.85 (Robinson, 1970). The diffuse radiation into the snowpack is

$$D = I_o(1-\alpha_s)\left\{\left[\psi_{O_3}(1-\psi_{rs})/2\right] + \left[\psi_{O_3}(1-\psi_{rs}) - (1-\psi_w)\right]\right.$$

$$\left.\psi_{da}(1-\psi_{ds})0.85\right\}\psi_C V_f F_s \qquad \text{(A.3)}$$

where V_f is the pixel view factor, which represents the fraction of the pixel open to the sky hemisphere.

The reflected radiation is an infinite sum of reflected radiation between sky and atmosphere. However, it is only of significance in this study when there is cloud cover and only one return is considered. This is estimated as

$$R = (I+D)\alpha_s(1-\alpha_s)\alpha_c V_f^{\,2} F_s^{\,2} \qquad \text{(A.4)}$$

A.2 Longwave radiation

The longwave radiation term consists of four components: emissions from the atmosphere, clouds, forest, and snow surface. As with the shortwave component, the effect of the surface radiation from neighboring pixels is neglected, which is an appropriate assumption in the presence of forest cover. Longwave radiation is partitioned between forest-snow exchange and atmosphere-snow exchange. The longwave radiation balance at the surface is

$$Q_L = (Q_{La} + Q_{Lc})V_f(1 - F) + Q_{Lf}F - Q_{Ls} \tag{A.5}$$

where F is the fractional forest cover. The atmospheric component is

$$Q_{La} = \varepsilon_a \sigma T_a^4 \tag{A.6a}$$

the cloud component (Kimball et al., 1982) is

$$Q_{Lc} = \sum_{i=1}^{n} \tau_8 f_8 \varepsilon_{c_i} \sigma T_{c_i}^4 \tag{A.6b}$$

the forest component is

$$Q_{Lf} = \varepsilon_f \sigma T_f^4 \tag{A.6c}$$

and the surface component is

$$Q_{Ls} = \varepsilon_s \sigma T_s^4 \tag{A.6d}$$

where ε is emissivity, σ is the Stefan-Boltzmann constant, T is temperature, and τ_8 and f_8 are the transmissivity and fraction of radiation in the 8–14 μm band, the region where the atmosphere is opaque in the infrared. The subscripts a, c_i, f, and s represent air, cloud at level i, forest, and snow, respectively.

A.3 Heat transfer

A bulk aerodynamic formulation (Sellers, 1965; Deardorff, 1968) is used for sensible heat:

$$Q_H = \rho_a c_p C_H u_a F_u (T_a - T_s) S_f \tag{A.7}$$

and for latent heat:

$$Q_E = \frac{0.622 \rho_a L_s}{P_a} C_W u_a F_u (e_a - e_s) S_f \tag{A.8}$$

where C_H and C_W are the bulk transfer coefficients for heat and water, which depend on wind reference height, u_a is the near-surface wind speed (e.g., at elevation 10 m above the surface), P_a is the atmospheric pressure, F_u is an adjustment factor for the forest effect on windspeed, e is the vapor pressure, c_p is the specific heat, L_s is the latent heat of sublimation, ρ_a is the air density, and S_f is a stability adjustment.

Appendix B

As seen in Section 4B, the mathematical description of the DMRT involves integro-differential equations that must be solved numerically and an inverse relationship that is difficult to estimate. There are several methods available to determine the inverse. We have chosen to use a neural network representation of the DMRT to solve the inverse problem. The input-output pairs of the DMRT are used to train the neural network . Once the neural network is trained, the brightness temperatures can be computed readily from the input parameters S. This has been used for the DMRT in Tsang et al. (1992) and Davis et al. (1993). We use a multilayer perceptron (MLP) which is a feedforward neural network having one or more layers of hidden neurons between the input and output layers. They have a simple layer structure, where successive layers of neurons are fully interconnected, with the connecting weights controlling the strength of the connections. Based on the snowpack parameters S as the inputs and brightness temperatures $\mathbf{T_b}$ as the outputs, the MLP has four separate input and output nodes. We used one hidden layer with five nodes. The MLP is a representation of the function ϕ where $\mathbf{T_b} = \phi(\mathbf{S}, \mathbf{F})$ as shown in Figure 12.

An MLP is a function determined by its architecture and its connection weight values. The input vector passes directly to the first layer of connection weights. The input $u_i(l+1)$ to each neuron in the next layer is the sum of all of its incoming connection weights multiplied by their connecting input neural activation value $a_j(l)$. The trainable offset value associated with the neuron is added to the sum, and the result is fed into the nonlinear function of the neuron, which is usually the sigmoid function (Lippmann, 1987),

$$f(u) = \left(1 + e^{-u}\right)^{-1}. \tag{B.1}$$

The training phase of the MLP uses the backpropagation (BP) learning rule, an iterative gradient descent algorithm designed to minimize the mean squared error between the desired targets and the actual output vectors. The weights are updated until a minimum error criterion is reached between the target values $\mathbf{T}_b$ and the predicted outputs from the MLP.

To provide a training set for the neural network, the DMRT is run for many combinations of the four snowpack parameters, discretizing the space appropriately. The neural network is trained on this model output set until the overall improvement at each new iteration becomes small.

This provides the forward model which outputs the 1 km pixel brightness temperatures, given the snow hydrology parameters. The adjusted brightness temperatures, based on the simulated and measured values are used as inputs to the inverted neural network, which then gives adjusted snowpack parameters for each 1 km pixel. The snow hydrology model then continues onward with these updated parameters, being updated for each day in which there are SSM/I observations available. A least mean square error scheme is used to update the snow parameters for each pixel using the neural network inversion of the DMRT. The snow hydrology model then continues forward with the updated parameters until the next SSM/I observation. This is the forward iterative inversion neural network technique discussed in Davis et al. (1993).

References

Anderson, J. R., E. E. Hardy, J. T. Roach, and R. E. Witmer, "A land use and land cover classification system for use with remote sensor data", *Professional Paper 964*, US Geological Survey, Washington, DC, 1976.

Bales, R. C., and R. F. Harrington, "Recent progress in snow hydrology", *Rev. Geophys.*, 33, Suppl., 1011–1020, 1995.

Baxter, R., "Ornstein-Zernike relation and Percus-Yevick approximation for fluid mixtures", *J. Chem. Phys.*, 52(9), 4559–4562, 1970.

Chang, A. T. C., J. L. Foster, and A. Rango, "Utilization of surface cover composition to improve the microwave determination of snow water equivalent in a mountain basin", *Int. J. Remote Sens.*, 12(11), 2311–2319, 1991.

Davies, J. A., and, S. B. Idso, "Estimating the surface radiation balance and its components", in *Modification of the Aerial Environment of Crops*, edited by B. J. Barfield and J. F. Gerber, 183–210, Amer. Soc. Agr. Eng., St. Joseph, MI, 1979.

Davies, J. A., W. Schertzer, and M. Nunez, "Estimating global solar radiation", *Bound. Layer Meteorol.*, 9(1), 33–52, 1975.

Davis, D. T., Z. Chen, L. Tsang, J.-N. Hwang, and A. T. C. Chang, "Retrieval of snow parameters by iterative inversion of a neural network", *IEEE Trans. Geosci. Remote Sens.*, 31(4), 842–852, 1993.

Davis, D. T., Z. Chen, J.-N. Hwang, L. Tsang, and E. Njoku, "Solving inverse problems by Bayesian iterative inversion of a forward model with applications to parameter mapping using SMMR remote sensing data", *IEEE Trans. Geosci. Remote Sens.*, 33(5), 1182–1193, 1995.

Deardorff, J. W., "Dependence of air-sea transfer coefficients on bulk stability", *J. Geophys. Res.*, 73(8), 2549–2557, 1968.

Dozier, J., and D. Marks, "Snow mapping and classification from Landsat Thematic Mapper data", *Ann. Glaciol.*, 9, 1–7, 1987.

Engman, E. T., Recent advances in remote sensing in hydrology", *Rev. Geophys.*, 33, Suppl., 967–975, 1995.

Hallikainen, M. T., and P. A. Jolma, "Comparison of algorithms for retrieval of snow water equivalent from Nimbus-7 SMMR data in Finland", *IEEE Trans. Geosci. Remote Sens.*, 30(1), 124–131, 1992.

Hollinger, J. P., J. L. Peirce, and G. A. Poe, "SSM/I instrument evaluation", *IEEE Trans. Geosci. Remote Sens.*, 28(5), 781–790, 1990.

Jordan, R., "A one-dimensional temperature model for a snow cover: Technical documentation for SNTHERM.89", *Special Rep. 91-16*, US Army Cold Regions Research Engineering Laboratory, Hanover, NH, 1991.

Josberger, E. G., and E. Beauvillain, "Snow cover of the Upper Colorado River Basin from satellite passive microwave and visual imagery", *Nordic Hydrol.*, 20, 73–84, 1989.

Kimball, B. A., S. B. Idso, and J. K. Aase, "A model of thermal radiation from partly cloudy and overcast skies", *Water Resour. Res.*, 18(4), 931–936, 1982.

Lippmann, R. P., "An introduction to computing with neural nets", *IEEE Acoust., Speech, Signal Processing Mag.*, 4(2), 4–22, 1987.

Marks, D., "Climate, energy exchange, and snowmelt in Emerald Lake watershed", Sierra Nevada, Ph. D. dissertation, University of California, Santa Barbara, 1988.

Munro, D. S., and G. J. Young, "An operational net shortwave radiation model for glacier basins", *Water Resour. Res.*, 18(2), 220–230, 1982.

Percus, J. K., and G. J. Yevick, "Analysis of classical statistical mechanics by means of collective coordinates", *Phys. Rev.*, 110(1), 1–13, 1958.

Rango, A., "Progress in developing an operational snowmelt-runoff forecast model with remote sensing input", *Nordic Hydrol.*, 19, 65–76, 1988.

Rango, A., "Snow hydrology processes and remote sensing", *Hydrologic Processes*, 7, 121–138, 1993.

Rango A., J. Martinec, A. T. C. Chang, J. L. Foster and V. F. van Katwijk, "Average areal water equivalent of snow in a mountain basin using microwave and visible satellite data", *IEEE Trans. Geosci. Remote Sensing*, 27(6), 740–745, 1989.

Robinson, G. D., "Some meteorological aspects of radiation and radiation measurement", *Adv. Geophys.*, 14, 285–306, 1970.

Sellers, W. D., *Physical Climatology*, Univ. Chicago Press, 1965.

Shi, J., and J. Dozier, "Inferring snow wetness using C-band data from SIR-C's polarimetric synthetic aperture radar", *IEEE Trans. Geosci. Remote Sens.*, 33(4), 905–914, 1995.

Tsang, L., "Passive microwave remote sensing of dense nontenuous media", *J. Electromag. Waves Applic.*, 1(2), 159–173, 1987.

Tsang, L., "Dense media radiative transfer theory for dense discrete random media with particles of multiple sizes and permittivities", *Progress in Electromagnetic Research 6*, 181–230, Elsevier, New York, 1992.

Tsang L., Z. Chen, S. Oh, R. J. Marks II, and A. T. C. Chang, "Inversion of snow parameters from passive microwave remote sensing measurements by a neural network

trained with a multiple scattering model", *IEEE Trans. Geosci. Remote Sens.*, 30(5), 1015–1024, 1992.

U.S. Geological Survey, "Land use and land cover digital data from 1:250,000- and 1:100,000-scale maps", Data Users Guide 4, Reston, VA, 1990.

Wang, J. R., P. E. O'Neill, T. J. Jackson, and E. T. Engman, "Multifrequency measurements for the effects of soil moisture, soil texture, and surface roughness", *IEEE Trans. Geosci. Remote Sens.*, GE-21(1), 44–51, 1983.

Wang, J. R., A. T. C. Chang, and A. K. Sharma, "On the estimation of snow depth from microwave radiometric measurements", *IEEE Trans. Geosci. Remote Sens.*, 30(4), 785–792, 1992.

West, R., L. Tsang, and D. P. Winebrenner, "Dense medium radiative transfer theory for two scattering layers with a Rayleigh distribution of particle sizes", *IEEE Trans. Geosci. Remote Sens.*, 31(2), 426–437, 1993.

Wilson, L. L., L. Tsang, and J.-N. Hwang, "Mapping snow properties for spatially distributed snow hydrological modeling in mountainous areas using passive microwave remote sensing data", *Proceedings of the IEEE International Geoscience and Remote Sensing Symposium (IGARSS '96)*, Vol. I, 130–132, Lincoln, NE, May 1996.

Table 1. Data inputs used and from where they were obtained.

Data Type	Agency	Address
a) *Hydrology model inputs*		
Digital Elevation Model file	U. S. Geological Survey	Sioux Falls, SD
Land Use and Land Cover files	U. S. Geological Survey	Sioux Falls, SD
Hourly point meteorological measurements	National Weather Service	Asheville, NC
Daily precipitation totals	National Weather Service	Asheville, NC
Basin streamflow measurements	U. S. Geological Survey	Sioux Falls, SD
b) *Satellite remote sensing measurements*		
SSM/I microwave brightness temperatures	Marshall Space Flight Center, NASA	Huntsville, AL
c) *Ground truth measurements for algorithm validation*		
SNOTEL SWE measurements	Natural Resources Conservation Service	Portland, OR

Table 2. Name, location, and elevation of the SNOTEL stations available for the year of study that are in or near the basin (see Figure 2).

Number	Name	Latitude (Deg-Min)	Longitude (Deg-Min)	Elevation (m)
1	Beartown	37-43	107-30	3530
2	Middle Creek	37-37	107-02	3420
3	Slumgullion	37-59	107-12	3470
4	Upper Rio Grande	37-43	107-15	2860
5	Upper San Juan	37-29	106-50	3080
6	Wolf Creek Summit	37-29	106-48	3345

Table 3. The values used for the fixed parameter vector **F** in the DMRT for SNOTEL station #2 and for station #4.

Number	ε_g	T_g	Q	Q_g	g_{max} (cm)
2	$(3.0+i0.1)\varepsilon_0$	270.	0.40	0.25	0.0375 0.0450 0.0600
4	$(3.0+i0.1)\varepsilon_0$	270.	0.40	0.30	0.0350 0.0425 0.0500

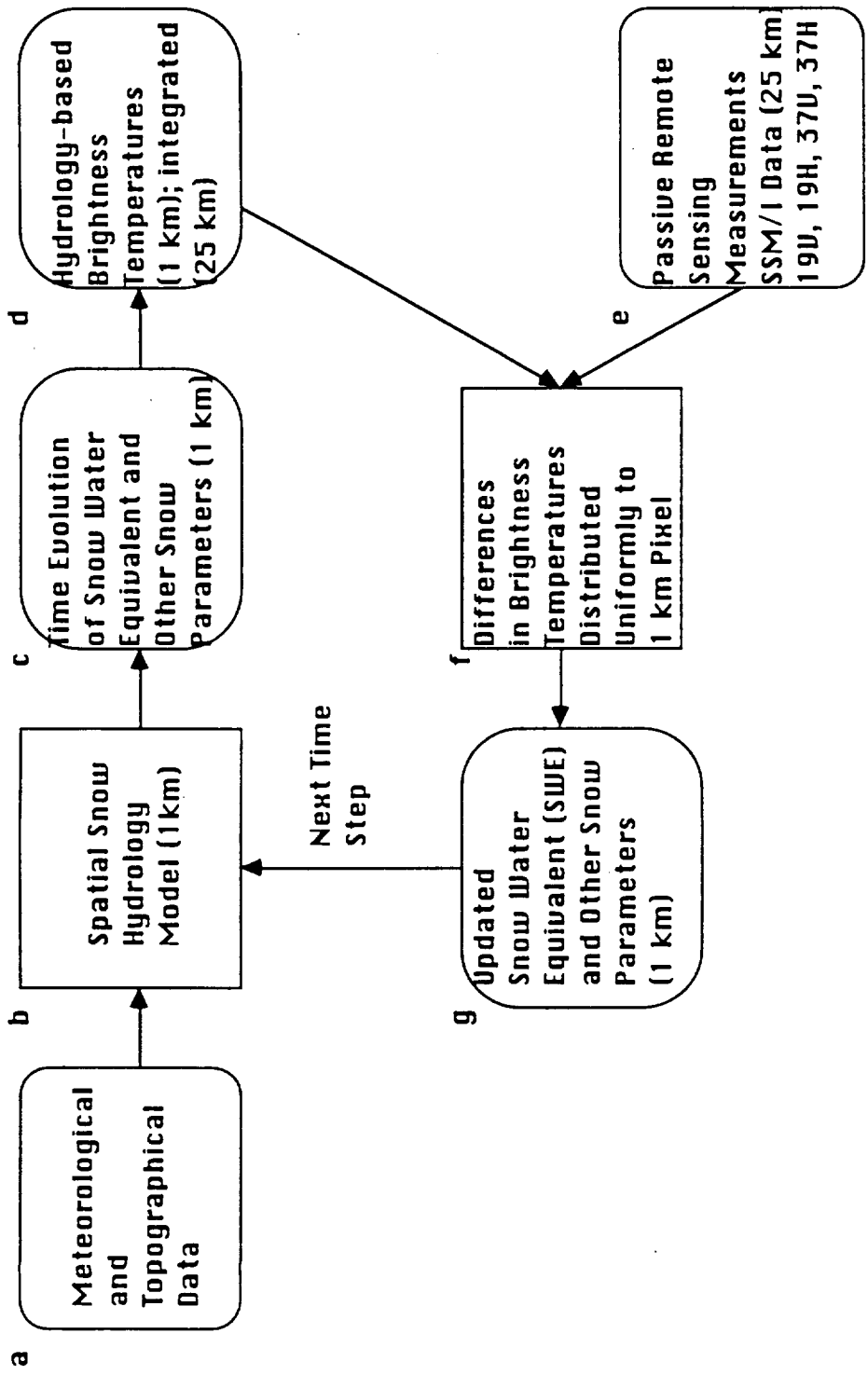

Figure 1 Flow chart outlining the steps in the combination of the snow hydrology model and remote sensing information to estimate snowpack parameters. Letters refer to paragraphs in the text.

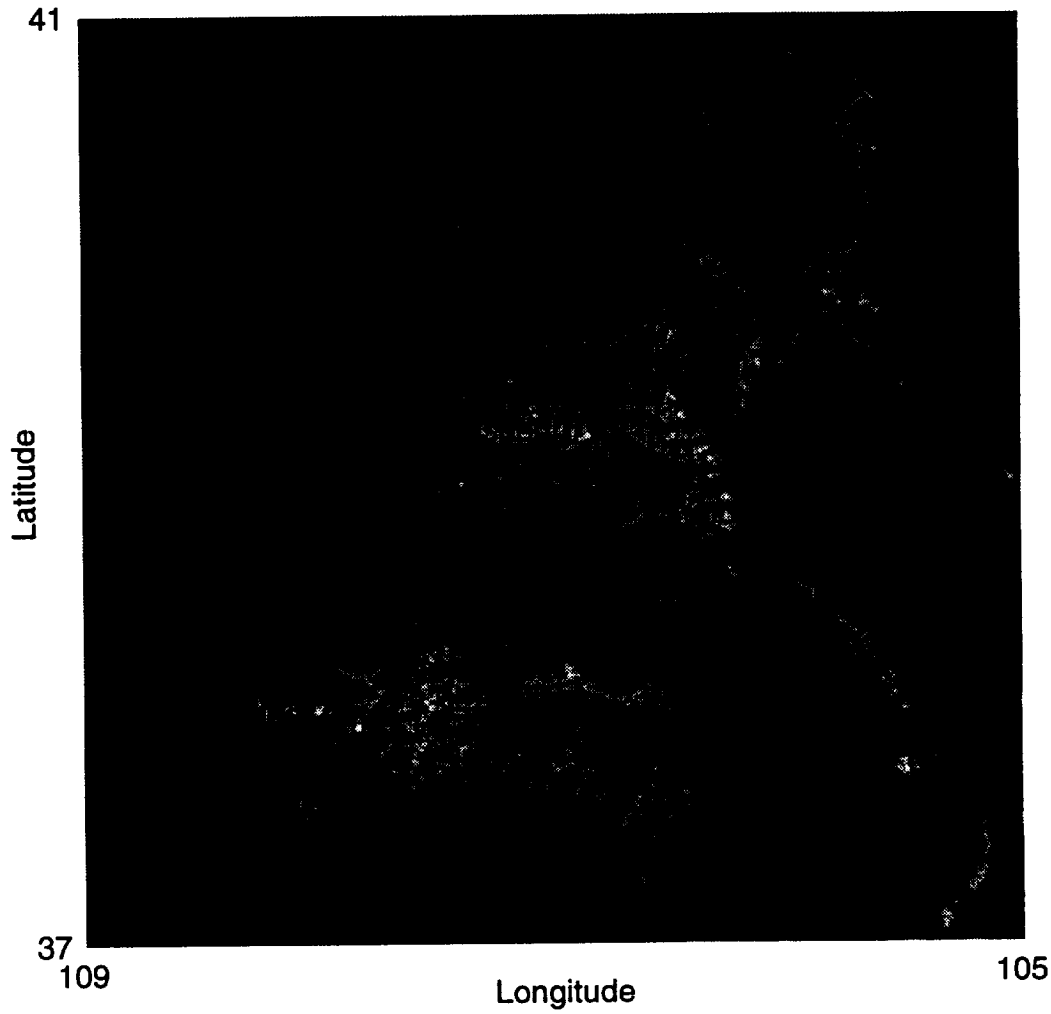

Figure 2 Location of the upper Rio Grande river basin near Del Norte, CO within the region. The left border is the boundary between Utah and Colorado, and the lower border the boundary between New Mexico and Colorado.

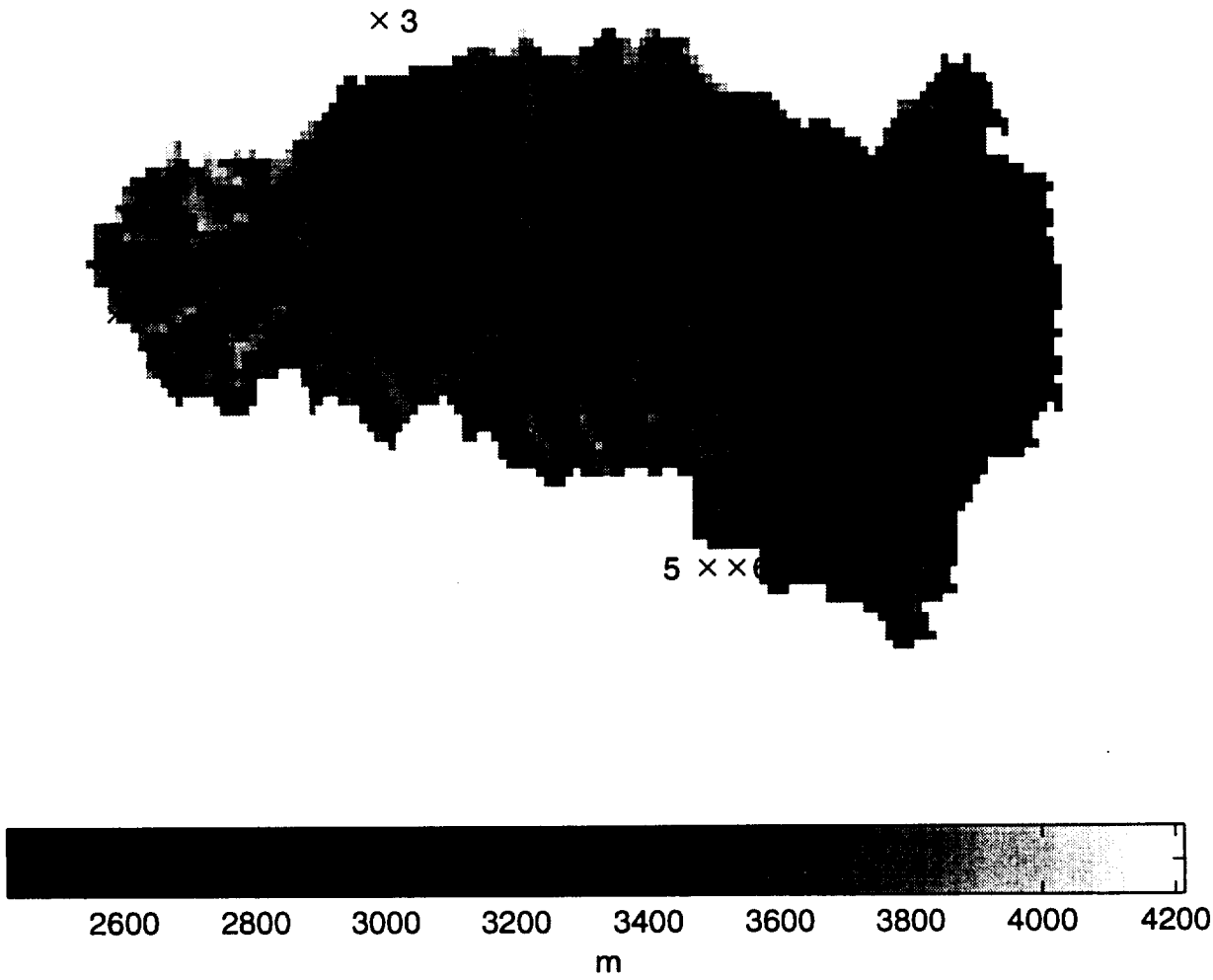

Figure 3 Elevation image of the Upper Rio Grande river basin near Del Norte, CO. The image resolution is 1 km based on the DEM. The location of the SNOTEL measurement stations are also included (see Table 1).

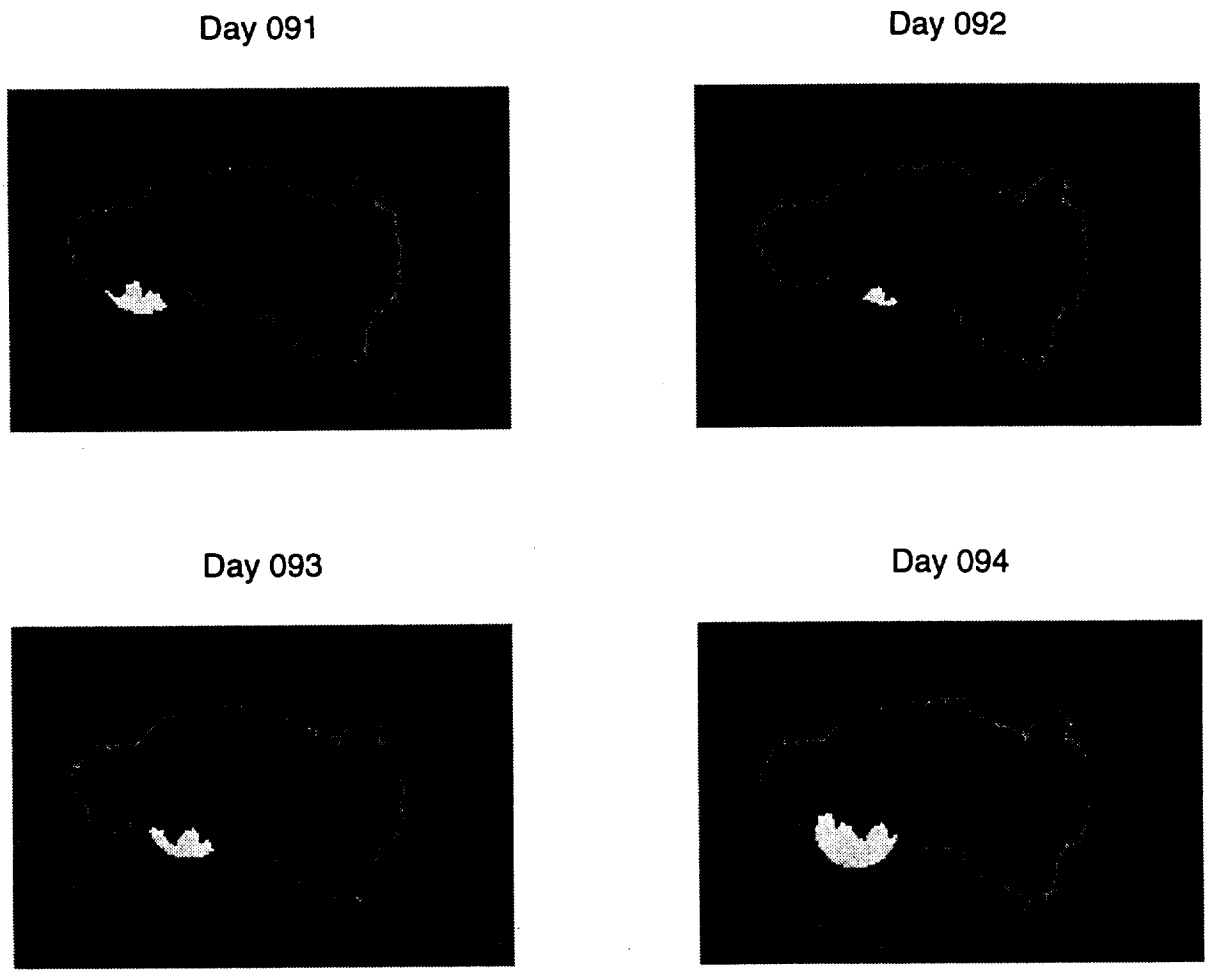

Figure 4 Sensor footprint coverage of a SNOTEL site for four consecutive days. The day-to-day variation in the coverage position of the footprint for the SNOTEL pixel is shown.

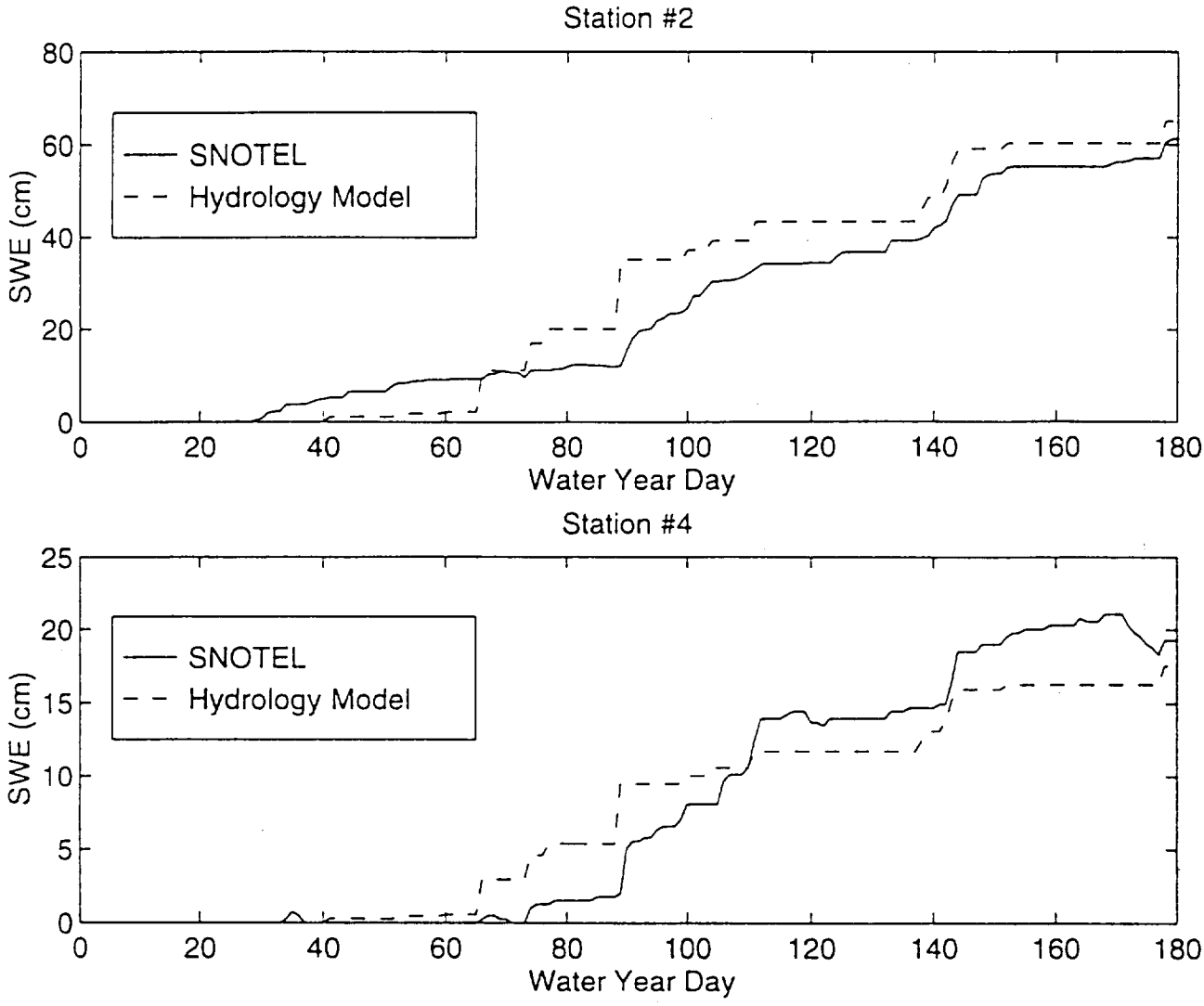

Figure 5 Comparison between hydrology model pixel simulated SWE and measured SWE for SNOTEL stations #2 and #4.

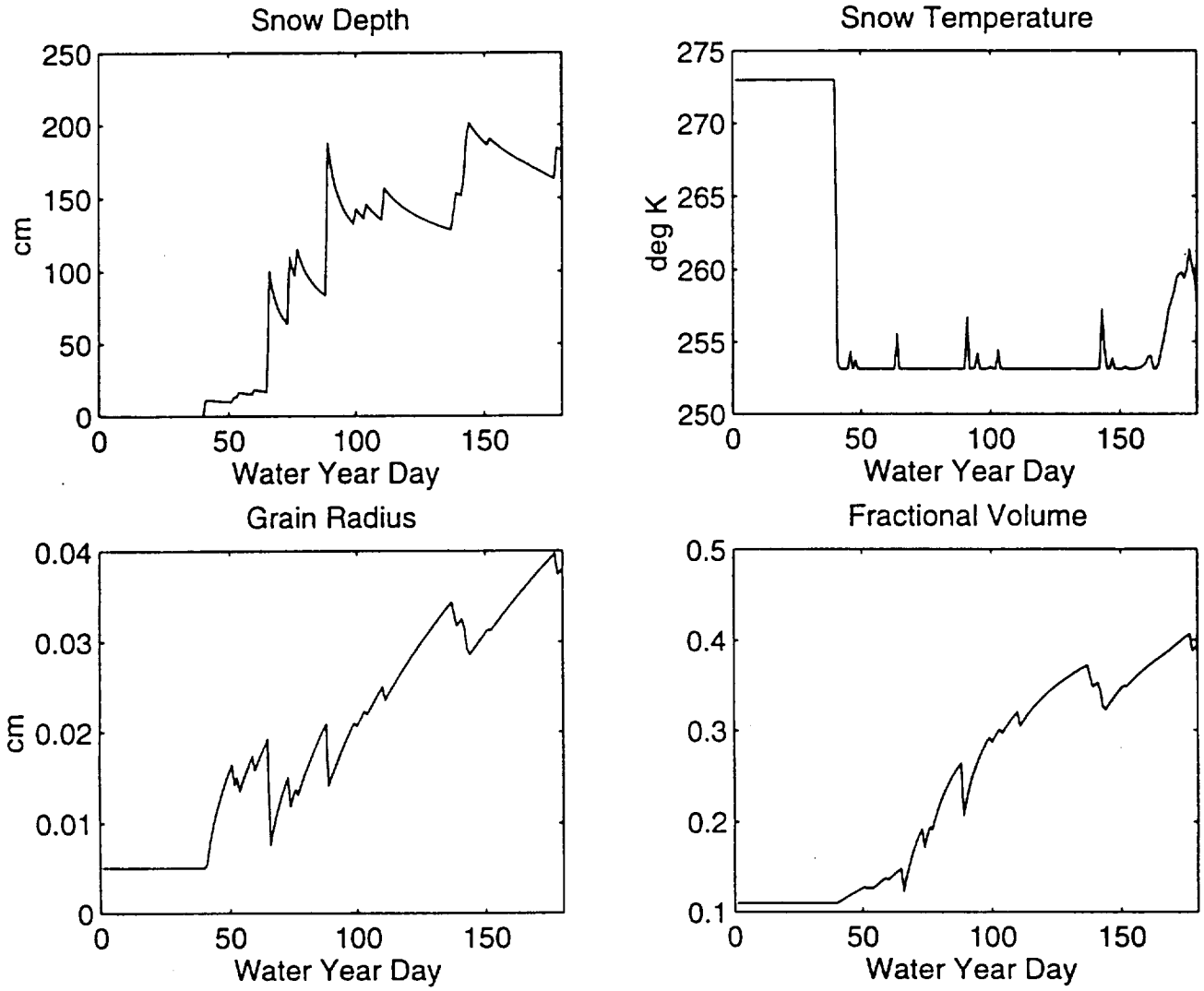

Figure 6a–d Evolution in time at station #2, high elevation station, of the four snowpack state variables in S: depth, temperature, grain size, and fractional volume.

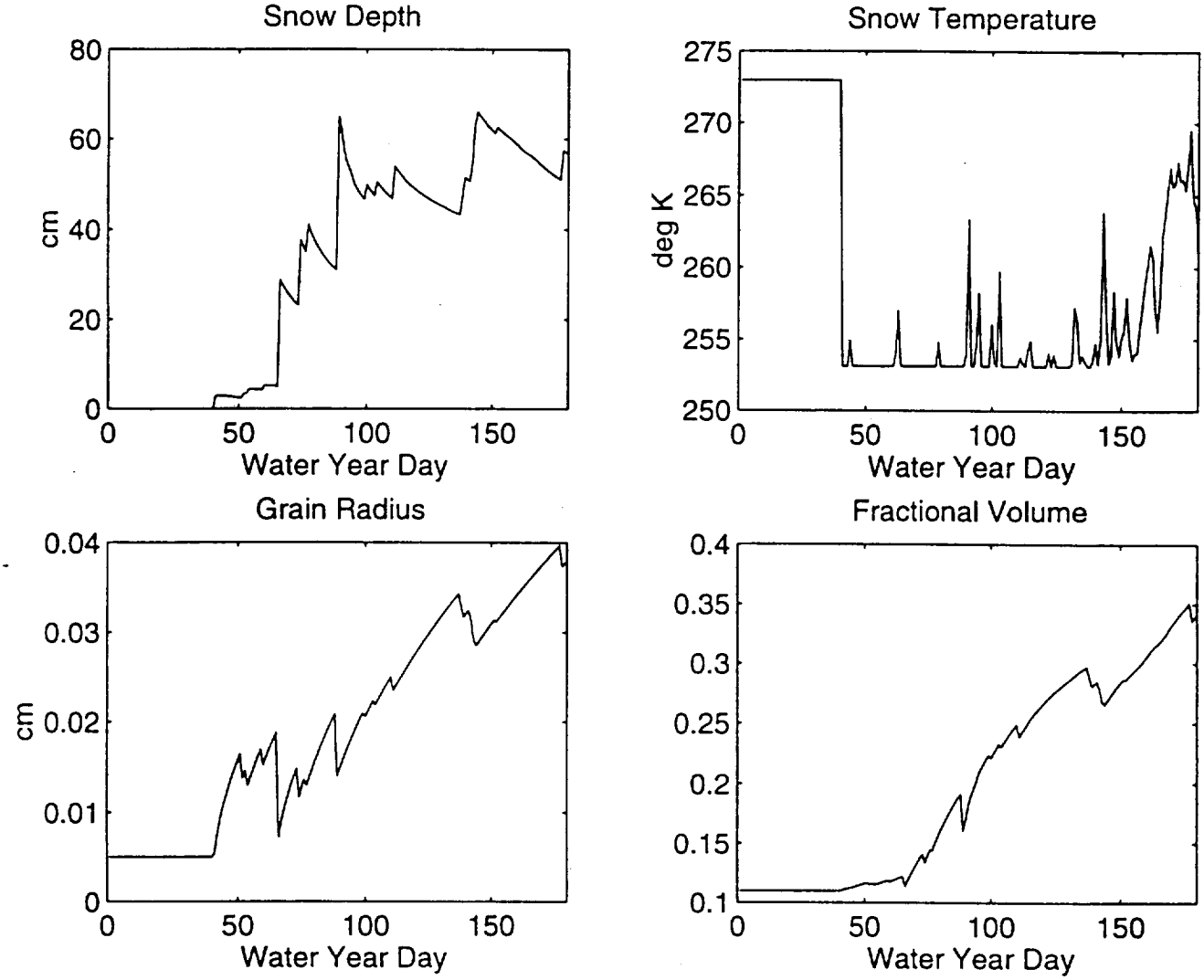

Figure 7a–d Evolution in time at station #4, low elevation station, of the four snowpack state variables in S: depth, temperature, grain size, and fractional volume.

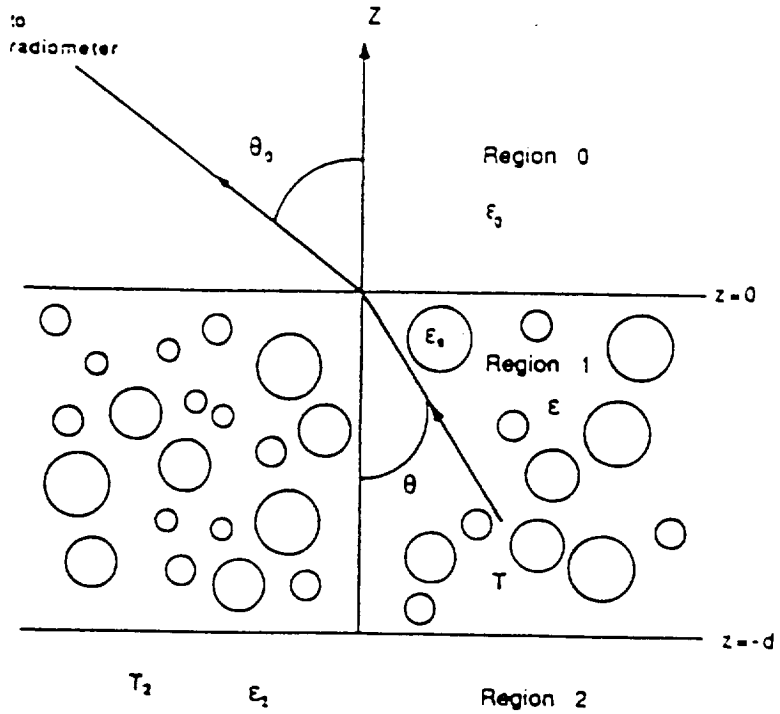

Figure 8 Passive remote sensing with observation of brightness temperatures of a layer of dielectric particles embedded in a background medium of permittivity ε overlaying a homogeneous half-space of dielectric medium of permittivity ε_2.

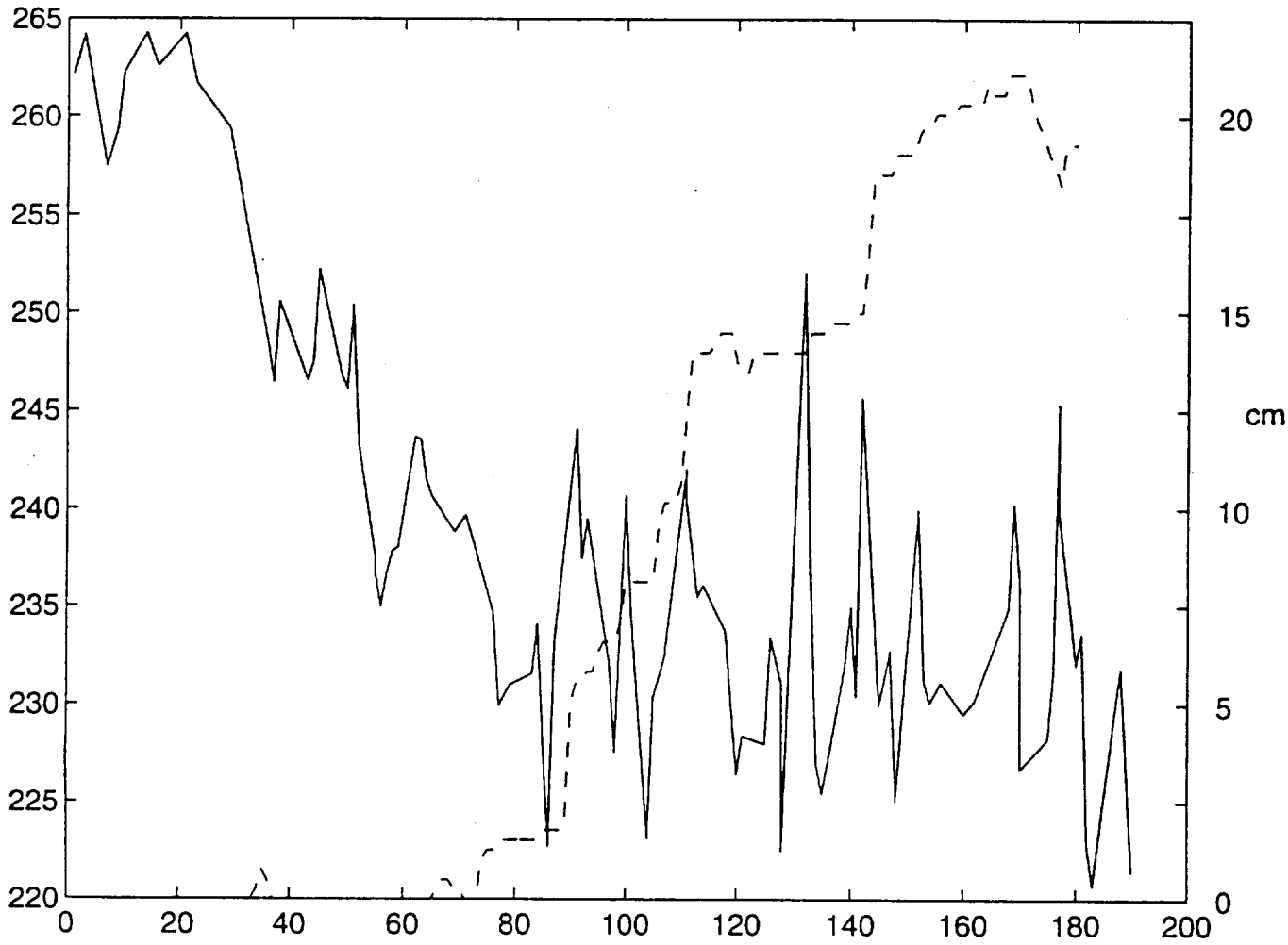

Figure 9a The 37 V brightness temperature plotted as a function of SNOTEL SWE for station #4 using a coverage radius of 12.5 km. This includes all brightness temperature measurements whose footprint covers the SNOTEL pixel.

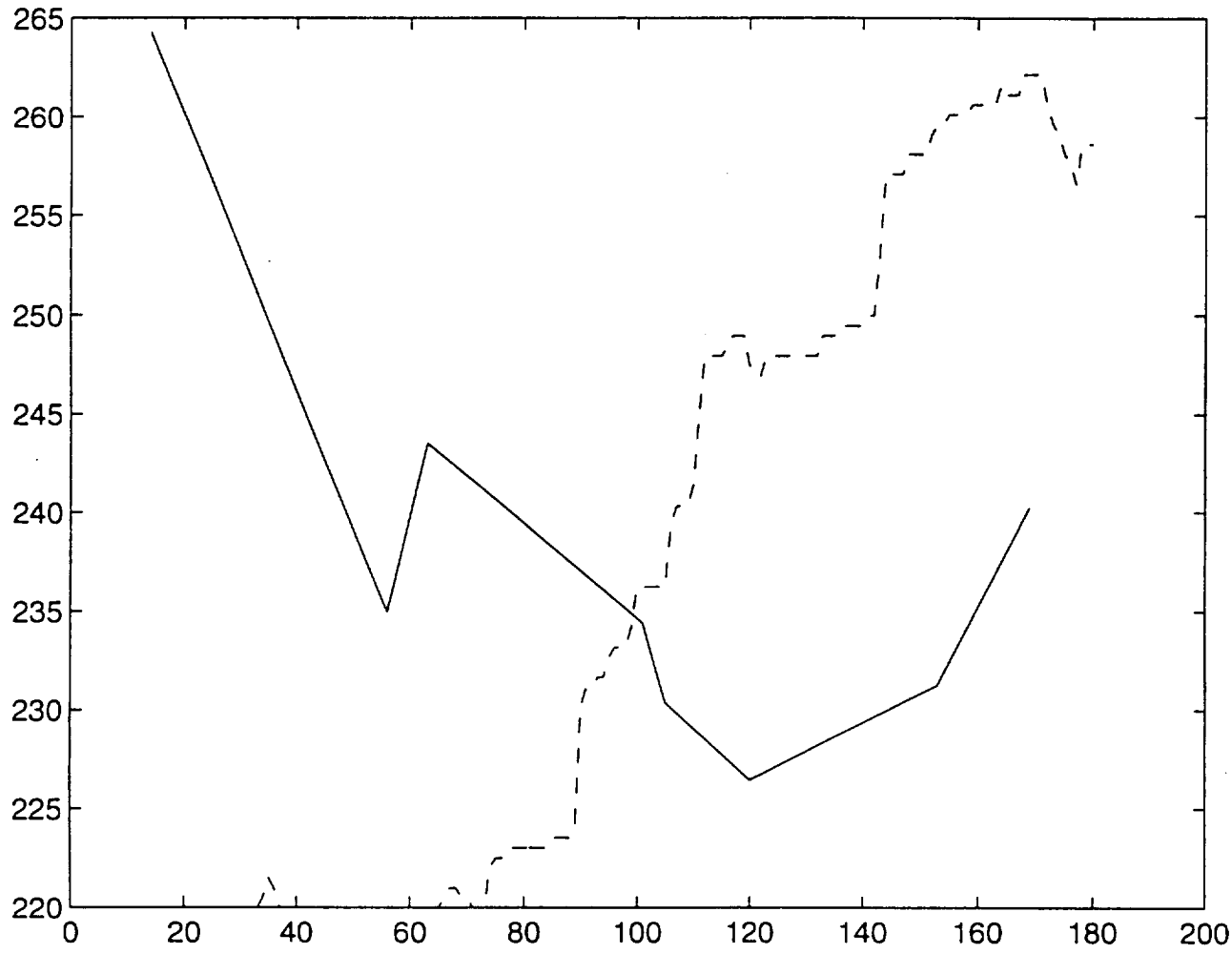

Figure 9b The 37 V brightness temperature plotted as a function of SNOTEL SWE for station #4 using a coverage radius of 4.0 km. The inverse relationship between brightness temperature and SWE is much clearer.

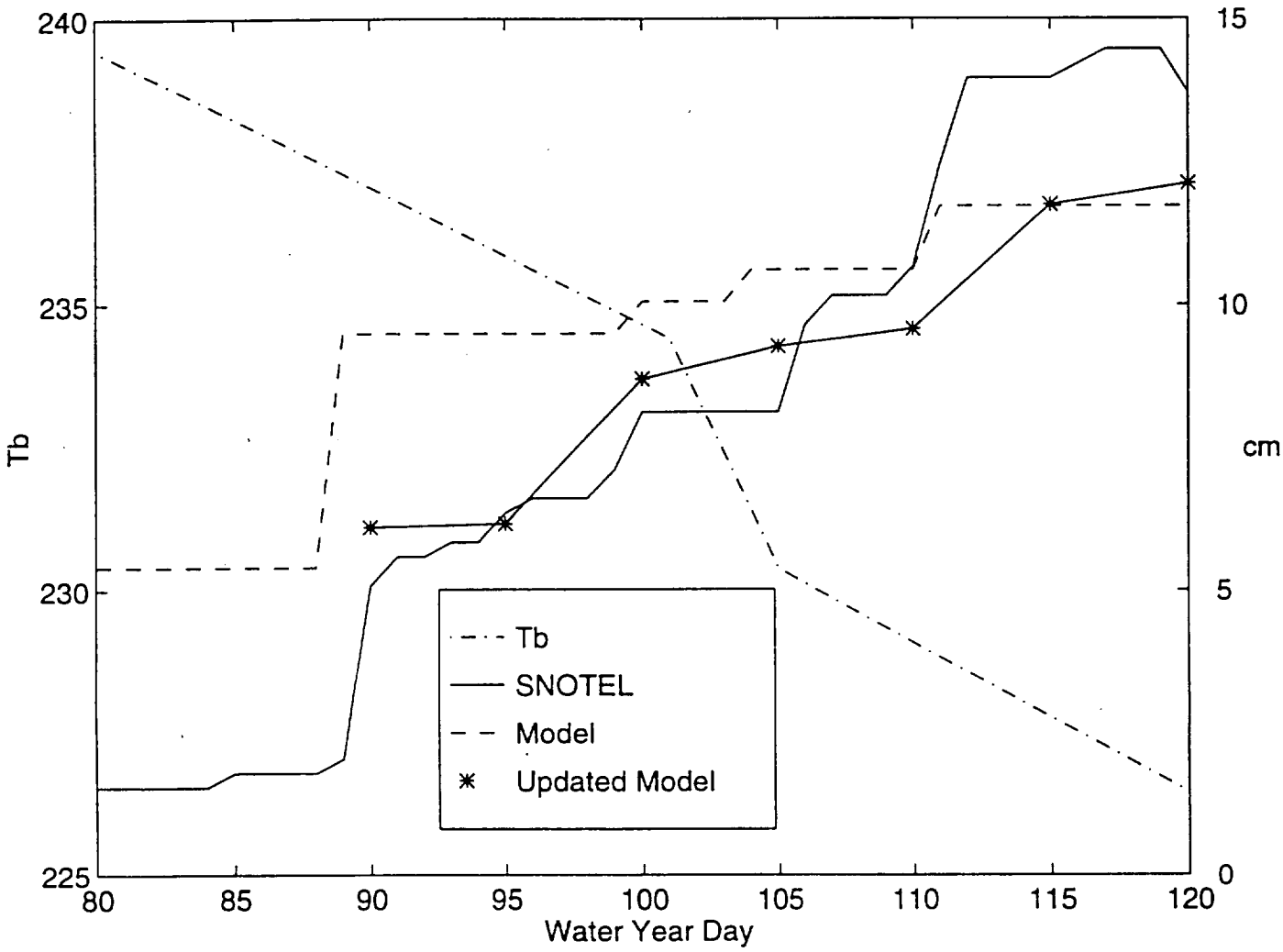

Figure 10 Comparison of the SWE simulations at SNOTEL station #4 for the hydrology model without updating and the hydrology model with updating. Four brightness temperature channels are used in the multi-parametric inversion. The 37 H brightness temperature measurements are shown for reference.

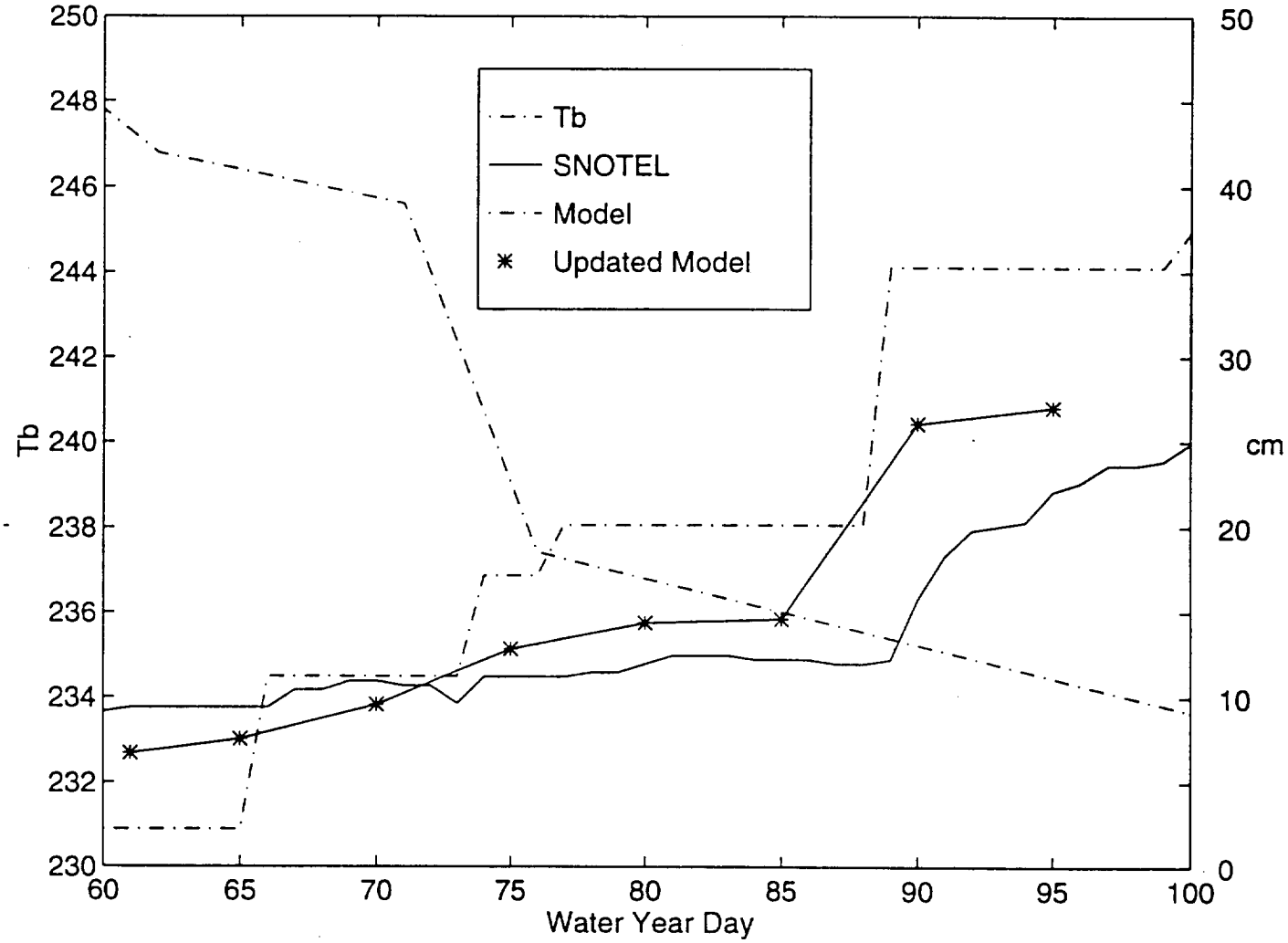

Figure 11 Comparison of the SWE simulations at SNOTEL station #2 for the hydrology model without updating and the hydrology model with updating. Four brightness temperature channels are used in the multi-parametric inversion. The 37 H brightness temperature measurements are shown for reference.

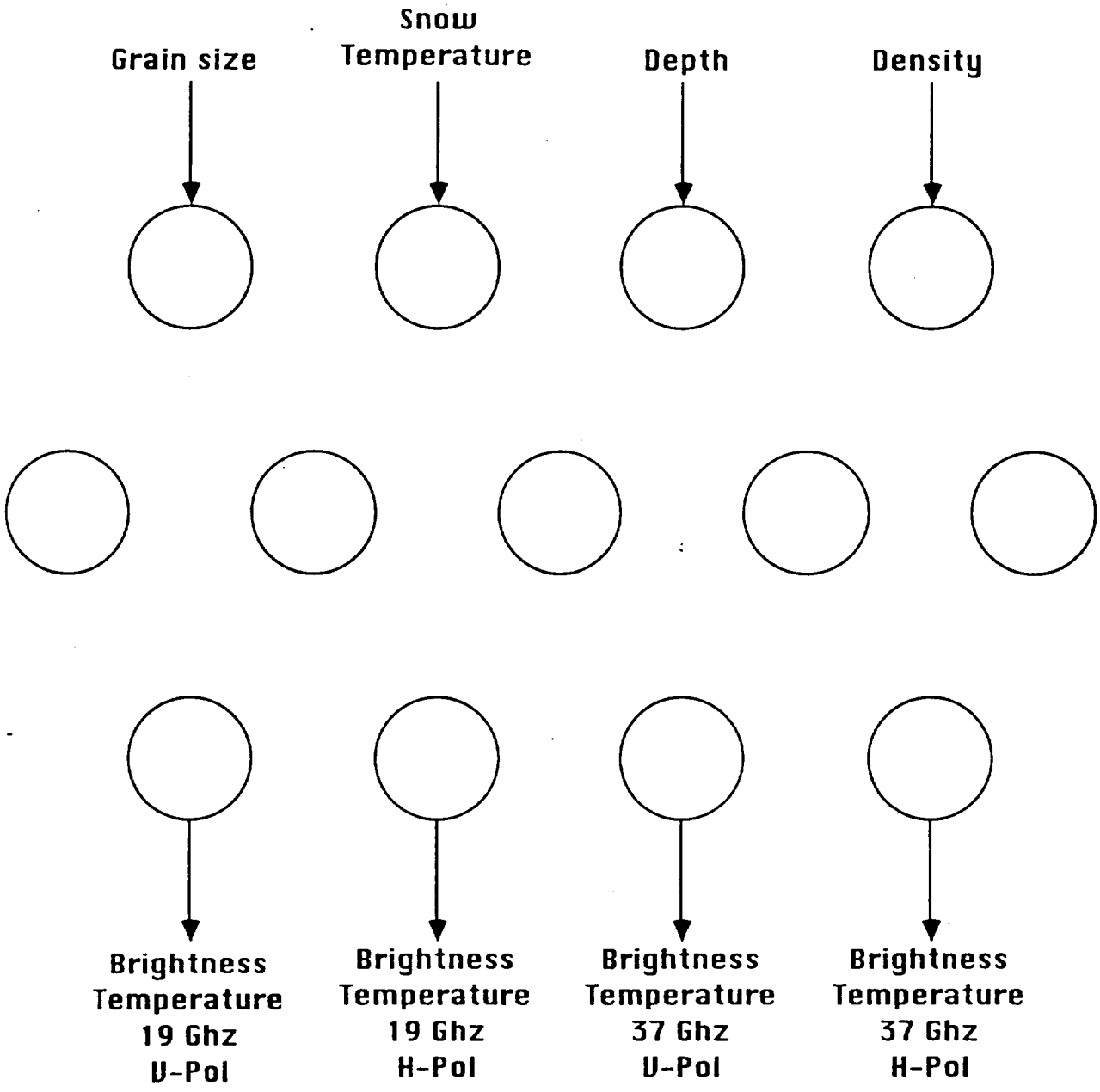

Figure 12 The structure of the multilayer perceptron neural network used to represent the dense medium radiative transfer model (DMRT). We use four input nodes, four output nodes, representing the input and output vectors $\mathbf{S}$ and $\mathbf{T_b}$, and one hidden layer with five nodes.